PAPER

A Model Optimization Approach to the Automatic Segmentation of Medical Images

Ahmed AFIFI[†], *Nonmember*, **Toshiya NAKAGUCHI**[†], **Norimichi TSUMURA**[†], *and* **Yoichi MIYAKE**[†,††], *Members*

SUMMARY The aim of this work is to develop an efficient medical image segmentation technique by fitting a nonlinear shape model with pre-segmented images. In this technique, the kernel principle component analysis (KPCA) is used to capture the shape variations and to build the nonlinear shape model. The pre-segmentation is carried out by classifying the image pixels according to the high level texture features extracted using the over-complete wavelet packet decomposition. Additionally, the model fitting is completed using the particle swarm optimization technique (PSO) to adapt the model parameters. The proposed technique is fully automated, is talented to deal with complex shape variations, can efficiently optimize the model to fit the new cases, and is robust to noise and occlusion. In this paper, we demonstrate the proposed technique by implementing it to the liver segmentation from computed tomography (CT) scans and the obtained results are very hopeful.

key words: *model fitting, image segmentation, kernel methods, prticle swarm, shape priors*

1. Introduction

The image segmentation is the first and essential process in many medical applications including analysis of anatomical structure [1], lesion detection [2], volume measurement and surgical planning [3]. This process is traditionally performed by radiologists or medical specialists who use their knowledge and experience to manually trace the objects on each image or slice. In almost all of these applications, the medical specialists have to access a large number of images which is a tedious and a time consuming process. Although the automatic segmentation is helpful in these applications, it is a demanding issue which needs a considerable amount of knowledge inclusion.

Many researchers make an effort to develop semi-automatic and automatic medical image segmentation techniques and several articles have been presented in the literature. Some of these techniques interpret the image as an undirected and weighted graph, and compute the minimal cost path between user defined seed points [4]. Although this class of segmentation techniques gives the user a full control over the segmentation process, it still requires the user interaction time and the quality of segmentation result is greatly depends on the skills of the operator. Another class of these techniques depends on the gray levels analysis and a simple or iterative thresholding to create a binary images that are usually further processed by morphological operators to separate the attached organs [5]. The techniques of this class are likely to fail when the gray levels of different organs are similar or when patients with completely different gray level characteristic are processed. To overcome these limitations, a group of researchers used the learning techniques as the neural network to learn the gray level characteristics corresponding to different tissues [6]. Unfortunately their techniques are keeping some of the original limitations and they recommend the practice of basic anatomical knowledge.

Due to the limitation of the previously mentioned techniques, more advanced techniques incorporate the prior information captured from a set of training cases in the segmentation process [7]. These techniques capture and describe prior information regarding the shape, size and position of each organ. In order to achieve this goal the researches employ deformable models, statistical shape models, and probabilistic atlases [8]. However these techniques surmount the main limitations of previously mentioned techniques they produce their own limitations as the difficulty to build a proper training set, the challenge of representing all the shape variations, and the difficulty to get the optimal model parameters which fit the new cases. Moreover different approaches to medical image segmentation employ the level set method [9] with some novel speed functions. These methods propagate the implicitly defined surface toward the object boundary according to local image characteristic and the past front history [10]. Though these techniques are able to produce a reasonable segmentation, the reliance on image information alone often lead to inaccurate segmentation results and the incorporation of prior knowledge and the parameters adjustment can greatly affect their accuracy .

The incorporation of shape priors with the segmentation techniques has been shown to be an effective way for knowledge inclusion and it is leading to more robust segmentation [11]. Many researchers integrate linear shape priors with level set methods to control the contour evolution process [12]. However these approaches are able to capture small variations of the shape of an object, they lead to unrealistic shape priors when the object undergoes complex or nonlinear deformations. In [13], Y. Rathi, et. al proved that the nonlinear shape prior obtained from kernel PCA (KPCA) space is more realistic and outperform the linear one. Additionally in [14], S. Dambreville, et. al incorporated the nonlinear shape model into a level set framework. However these techniques incorporate nonlinear shape pri-

Manuscript received 00, 0000.
Manuscript revised 00, 0000.
Final manuscript received 00, 0000.

[†]Graduate School of Advanced Integration Science, Chiba University
[††]Research Center for Frontier Medical Engineering, Chiba University

ors, they depend on the variational level set method and they can be trapped in a local minima and a manual initialization is very essential. Furthermore, they rely on the image moments only which is unsatisfactory in the case of complex textures.

Therefore in this work, we propose an efficient automatic segmentation technique by combining texture features-based classification and nonlinear shape model optimization. In this technique, the high level texture features extracted using the over-complete wavelet packet decomposition are used to accurately define the different tissues and to perform a preliminary segmentation. Additionally, the kernel PCA (KPCA) is utilized to capture the shape variations and to build a nonlinear shape model from a set of manually segmented images. The particle swarm optimization algorithm (PSO) is then applied to efficiently obtain the parameters of the shape model and to accurately fit it with the pre-segmented images.

After this introduction, in Section2, the basic PSO algorithm is explained. In Section3, we briefly describe the KPCA and how it is used to obtain the nonlinear shape priors. The texture prior extraction will be discussed in Section4. In Section5, the proposed PSO segmentation framework will be presented. The experimental results will be shown in Section6 and the paper will be concluded in Section7.

2. Particle Swarm Optimization (PSO)

PSO is a population based stochastic optimization technique founded by Kennedy and Eberhart in 1995 [15]. In this algorithm they mimic the social behavior of bird flocks searching for food to produce computational intelligence. There are many similarities between PSO and the other evolutionary computation techniques, but the PSO algorithm supports the idea of individuals cooperation instead of competition used in the other techniques and that provides a better search methodology and reduces the dependency on the parameters initialization. Additionally, it can achieve better results in a faster and cheaper way compared with other evolutionary computational techniques as proved in [16] and as we will clarify in the experimental results.

In PSO, a population or swarm of individuals – particles – are separated over the search space of some problem. Each particle represents a complete solution of this problem and it evaluates the objective function at its location. Additionally, the particle moves in the search space under the influence of its behavior and the whole swarm behavior. Each particle in the swarm is defined by three $d-$dimensional vectors; the current location $\vec{x_i}$, the velocity $\vec{v_i}$ and the best position it reaches $\vec{p_i}$, where d is the dimensionality of the search space. The original version of PSO algorithm will be described in the following algorithm.

1. The position and velocities are randomly initialized from the specified range.
2. *loop*
   a. For each particle, evaluate the desired optimization fitness function.
   b. Compare particle's fitness evaluation with its $pbest_i$, where $pbest_i$ is the fitness evaluation at particle's best location. If current value is better than $pbest_i$, then set $pbest_i$ equal to the current value, and $\vec{p}_i$ equal to the current location $\vec{x}_i$.
   c. Identify the particle in the neighborhood with the best success so far, and assign its index to variable g.
   d. Change the velocity and position of each particle according to the following equations.

$$\begin{aligned} v_i^{\vec{t+1}} = v_i^{\vec{t}} &+ \vec{U}(0,\alpha_1) \otimes (\vec{p_i} - \vec{x_i}) \\ &+ \vec{U}(0,\alpha_2) \otimes (\vec{p_g} - \vec{x_i}) \end{aligned} \tag{1}$$

$$x_i^{\vec{t+1}} = \vec{x_i^t} + \vec{v_i^t}, \tag{2}$$

   where

   - t : reefers to the iteration index.
   - $\vec{U}\left(0,\alpha_j\right), j = 1,2$: represents a vector of random values uniformly distributed in $\left[0,\alpha_j\right]$.
   - v_i is kept within the range $[-V_{max}, +V_{max}]$.

   e. If a criterion is met (sufficiently good fitness or maximum number of iteration), exit loop.
3. save the global best position as the problem solution.

This original PSO algorithm has been received many enhancements from its appearance till now [17]. The PSO with inertia weight [17], [18] is one from these enhancements which provides better control on the search space, so we are interested in it during this work. The following equations are the velocity and position update equations of the PSO with inertia weight.

$$\begin{aligned} v_i^{\vec{t+1}} = \omega v_i^{\vec{t}} &+ \vec{U}\,(0,\alpha_1) \otimes (\vec{p_i} - \vec{x_i}) \\ &+ \vec{U}\,(0,\alpha_2) \otimes \left(\vec{p_g} - \vec{x_i}\right) \end{aligned} \tag{3}$$

$$x_i^{\vec{t+1}} = \vec{x_i^t} + \vec{v_i^t}, \tag{4}$$

where, ω is the inertia weight

The researchers have found that the large value of ω allows the particles to perform extensive exploration and the small value of ω increases the chance to get local optima. So they have found that the best performance could be achieved by using a large value of ω (e.g., 0.9) at the beginning and gradually decrease it until reach another small value of ω. in addition, the velocity of each particle is kept within a specified range of $[-maximumvelocity, maximumvelocity]$.

3. Nonlinear Shape Priors

The nonlinear shape priors have been proven to be an efficient way for the representation of complex object deformation [13]. Additionally, the KPCA has been shown as a

predominant tool to extract nonlinear structure from a data set [14]. In the following subsections, we will briefly review the KPCA and how it is utilized to form the shape priors.

3.1 Kernel principle component analysis (KPCA)

To extract the nonlinear structure from a complex dataset, we have to map this dataset from an input space I to a feature space F through a nonlinear function φ. Usually, the dimension of this mapping is very high and may be infinite and it increases the computational cost. Therefore, the KPCA benefits from the kernel trick to perform PCA in the feature space without explicitly mapping the dataset [19]. The kernel is a function $k(.,.)$ such that, for all data points x_i, the kernel matrix $K(i,j) = k(x_i, x_j)$ is symmetric positive definite. In addition, the kernel function gives the inner product between two points in the feature space, i.e., $k\left(x_i, x_j\right) = \left\langle \varphi(x_i), \varphi(x_j) \right\rangle$.

Let $\tau = \{x_1, x_2, , x_N\}$ be a set of training data. The kernel trick can be used to obtain the eigenvectors in the feature space from the following Eigen decomposition:

$$HKH = U\Sigma U^T, \tag{5}$$

where H is the centering matrix defined as $H = I - \frac{1}{N}\mathbf{1}\mathbf{1}^T$, I is the $N\times N$ identity matrix, $\mathbf{1} = [1, 1, \ldots, 1]^T$ is $N\times 1$ vector, $U = [a_1, a_2, \ldots, a_N]$ with $a_i = [a_{i1}, a_{i2}, \ldots, a_{iN}]$ is the matrix containing the eigenvectors and $\Sigma = diag(\lambda_1, \lambda_2, \ldots, \lambda_N)$ contains the corresponding eigenvalues. Denote the mean of the $\varphi-$mapped data by $\bar{\varphi} = \frac{1}{N}\sum_i^N \varphi(x_i)$ and as described in [13], [14], [19], the centered map $\tilde{\varphi}$can be defined as:

$$\tilde{\varphi}(x_i) = \varphi(x_i) - \bar{\varphi} \tag{6}$$

The k^{th} orthonormal eigenvector of the covariance matrix in the feature space can then be computed as:

$$V_k = \sum_1^N \frac{a_{ki}}{\sqrt{\lambda_k}}\tilde{\varphi}(x_i) \tag{7}$$

In addition, the projection of the $\varphi-$image of a test point x onto the subspace spanned by the first n eigenvectors is given by:

$$P\varphi(x) = \sum_{k=1}^{n}\beta_k V_k + \bar{\varphi}, \tag{8}$$

where, β_k is the projection of $\varphi(x)$onto the k^{th} component and it is computed as:

$$\beta_k = \frac{1}{\sqrt{\lambda}}\sum_{i=1}^{N} a_{ki}\tilde{k}(x, x_i), \tag{9}$$

$\tilde{k}(.,.)$ is the centered kernel function and it is given by:

$$\begin{aligned}\tilde{k}(x,y) &= \langle\tilde{\varphi}(x), \tilde{\varphi}(y)\rangle \\ &= k(x,y) - \frac{1}{N}\mathbf{1}^T k_x - \frac{1}{N}\mathbf{1}^T k_y + \frac{1}{N^2}\mathbf{1}^T K\mathbf{1}\end{aligned} \tag{10}$$

with $k_x = [k(x, x_1), k(x, x_2), \ldots, k(x, x_N)]^T$

3.2 Shape Priors Using KPCA

As a first step in the shape modeling, a set of CT slices must be segmented manually and its corresponding level set have to be formulated. In order to simplify this process, we built an interactive system that allows the medical doctor to segment the objects by selecting some points around it and then, the cubic Spline interpolation [20] is employed to estimate the segmenting curve from these points as shown in Figure 1 (a). Additionally, the level sets which describe the segmented objects are formulated according to the following procedure.

1. Construct a binary mask from the segmenting curve with the value of 1 inside the curve and the value of 0 outside it.
2. Use the binary mask generated in the previous step to generate a mask with the value of -1 inside the object and the value of 1 outside it. This mask is regarded as a sign function and denoted as s as shown in Figure 1 (b).
3. Compute the Euclidian distance transform between each pixel and the segmenting curve and denotes it as D as shown in Figure 1 (c).
4. Formulate the level set function as $\Psi(x,y) = s(x,y)\cdot D(x,y)$ as shown in Figure 1 (d).

Furthermore, the process of shape modeling is completed according to the following algorithm:

1. Load the N level set functions $\Psi_i(x,y), i = 1, 2, \ldots, N$ which had been constructed from the training images .
2. Constructing a column vectors $\psi_i, i = 1, 2, \ldots, N$ consisting of M samples of each Ψ_i, $M = m_1 \times m_2$ is the image size,by stacking the m_2 columns of Ψ_i.
3. Defining the shape matrix S as $S = [\psi_1, \psi_2, \ldots, \psi_N]$.
4. Using the Gaussian kernel $k\left(\psi_i, \psi_j\right) = e^{-\frac{d^2(\psi_i,\psi_j)}{2\sigma^2}}$, with $\sigma^2 = \frac{1}{N}\sum_{i=1}^N \min_{j\neq i} d^2(\psi_i, \psi_j)$ to build the kernel matrix K.
5. Applying KPCA as described in the previous section and selecting the eigenvectors that have eigenvalues greater than one as a shape representation.

4. Texture Priors

We utilize the over-complete wavelet packet transform to extract the high-level feature vectors for each foreground pixel in the training images. As illustrated in Figure 2 the over-complete wavelet packet transform does not perform the down-sampling as in standard wavelet packet transform, so it ensures the translation invariance property which is indispensable for textural analysis. In addition, it provides robust texture features at the expense of redundancy [21]. Feature extraction using over-complete wavelet packet transform can extract all bandpass information about the texture. In this work, we extract the wavelet packet feature set according to the following procedure:

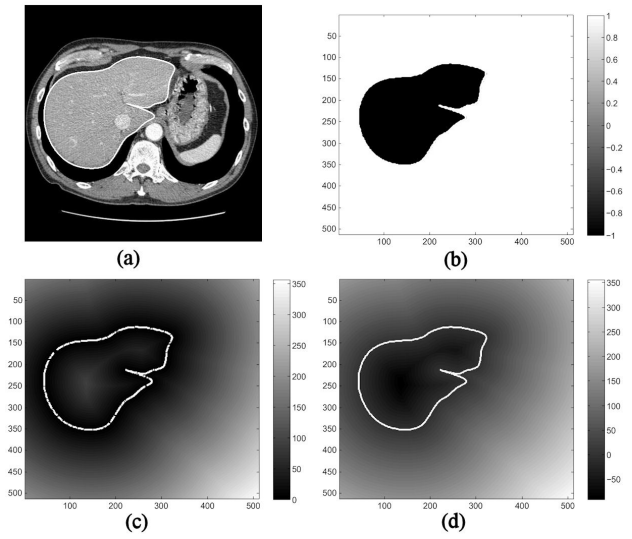

Fig. 1 Manual segmentation and level set formulation (a) the estimated curve, (b) the sign function s, (c) the distance function D, and (d) the signed distance function Ψ.

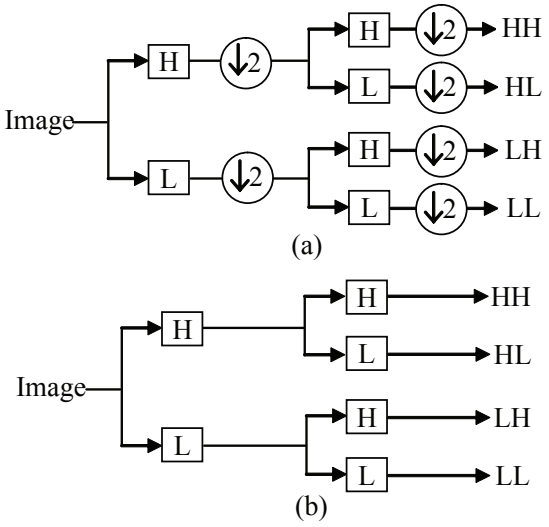

Fig. 2 Wavelet packet decomposition of an image into four sub-bands. (a) The standard decomposition, (b) The over-complete decomposition. H and L denote high-pass and low-pass filter respectively and ↓ 2 means a down-sampling by 2.

1. Apply a two-level over-complete wavelet packet decomposition on the input image.
2. At level−1, select the four sub-bands as feature sub-images.
3. At level−2, in each sub-channel, select the sub-band with the maximum variance to be a feature sub-image.
4. Calculate the local energy around each pixel of the feature sub-images as

$$E(x,y) = \frac{1}{2m+1} \sum_{i=-m}^{m} \sum_{j=-m}^{m} F\,(x+i, y+j)^2, \quad (11)$$

where, $F(x+i, y+j)$ is the wavelet coefficient of a feature sub-image in $(2m+1)\times(2m+1)$ window centered at pixel (x, y).

5. Construct the feature vectors of each pixel in the image from the energy of the corresponding feature sub-images.

After the construction of the high level feature vectors, we assign a label for each pixel to indicate whether this pixel is a desired object pixel or not and finally, we use the linear fisher discriminate algorithm [22] to build the textural prior model. The energy, $l_2 - norm$, of each feature sub-image is a favorable feature of texture because it indicates the dominant spatial-frequency channels of the original image and it leads to better classification results than the spatial domain methods as shown in Figure 3. Linear fisher discriminate algorithm is a classification method that project high-dimensional data onto a line and performs classification in this one-dimensional space. This projection maximizes the distance between the means of the two classes while minimizing the variance within each class.

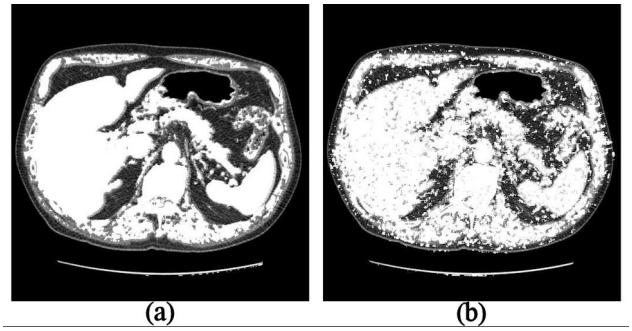

Fig. 3 Sample classification results, (a) using wavelet texture feature set and (b) using Laws texture.

5. PSO-Based Segmentation

In order to segment a new image, its wavelet packet based feature set is extracted and each foreground pixel in this image is classified as a desired object pixel (true) or undesired object pixel (false) according to the prior textural model as shown in Figure 4. This classification process is carried out by using the linear fisher discriminate algorithm. Finally, this stage is completed by applying the PSO algorithm [17] to get the level set function that truly segments the image as shown in Figure 5 and described in the following sections.

5.1 The Model Description

Each particle in the PSO population consists of the set of parameters that control the shape and the pose parameters of the segmenting curve. In this framework, the level set function $\phi(x, y)$ that implicitly represents the segmenting curve is defined as the pre-image of feature vector $\upsilon = \sum_{i=1}^{l} w_i \alpha_i, l$

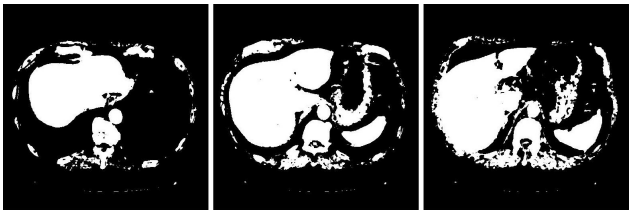

Fig. 4 Preliminary segmentation of sample images: the foreground is the pixels classified as desired object pixels.

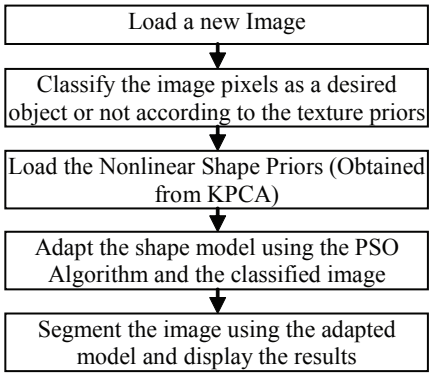

Fig. 5 The proposed segmentation technique

is the number of KPCA principle components, α_i and w_i, $i = 1, 2, \ldots, l$ are the normalized KPCA principle components and its weights respectively. The pre-image of this feature vector is computed according to the direct method proposed in [23].

Furthermore, we consider the pose parameters, a, b for transition, h for scaling and θ for rotation, which incorporated in this framework using an affine transform. According to above considerations, each individual, particle, P in the PSO population is defined as $P = [(w_i, i = 1, 2, , l), a, b, h, \theta]$ and it represents a segmenting curve.

The fitness of each particle in this work represents how the corresponding curve segments the image. Accordingly in the proposed framework, we tend to maximize the fitness function used in [24]. This fitness function is formulated as:

$$FT = 500\,(A + (1 - B))\,, \tag{12}$$

where, A is the fraction of pixels inside the segmenting curve that are labeled "true" and B is the fraction of the pixels outside the segmenting curve that are labeled "true". The maximization of this fitness function means that more desired pixels are gathered inside the segmenting curve.

5.2 The PSO algorithm configuration

In this work, we are employing the PSO algorithm with inertia weight described in Section1. The PSO algorithm includes an inertia term and acceleration constants which give us more control on the segmenting curve. The PSO algorithm configuration is shown in Table1 and the curve parameters configuration is provided in Table2. The parameters in Table1 control how fast the PSO converge to the correct segmentation and make the balance between the global and local search, however the PSO is robust to initialization. The parameters in Table2 control the shape formulation and its transformation. Among these parameters, w_i have fixed ranges and the other parameters are selected practically according to the characteristic of the cases and the selection of these parameters have to guarantee that all possible variations and transformations are considered.

5.3 The PSO Algorithm Implementation

After we configure the PSO algorithm and adjust the curve parameters according to the desired object, we carry out the segmentation process according to the following sequence:

1. Initialize the curve parameter randomly from the range specified in Table1.
2. Create the level set function from the curve parameters.
3. Segment the image by all segmenting curves derived from the level set.
4. Measure the fitness of each curve by computing the fitness function described in Section5.1.
5. Determine the best segmenting curve and the best segmentation results for each curve.
6. If the best curve is not changed for more than 30 iterations, produce the segmentation results; else go to Step-6.
7. Update the curves parameters according to the PSO algorithm equations and go to Step-2.

6. Experimental Results

In this work, we use a portal phase of computed tomography (CT) images of resolution 512×512 pixels and of 1mm slice interval to perform two experiments of liver segmentation. The used datasets contain normal cases as well as cases with liver abnormalities, tumors and cysts. In the first experiment, a set of five CT images of different patients were used. Each CT image consists of about 150 slices stacked together and the liver fully appears in about 100 slices. In this

Table 1 PSO algorithm configuration

Swarm size (the number of segmenting curves)	25
The maximum number of epochs	100
Local best influence	2
Global best influence	2
Initial inertia weight	0.9
Final inertia weight	0.4
Epoch when inertial weight at final value	70

Table 2 Curve parameter configuration

Parameter Name	Parameter Rang	Maximum Velocity
$w_i, i = 1, \ldots, l$	$-\sqrt{\lambda_i} \rightarrow \sqrt{\lambda_i}$	0.5
a, b	$-10 \rightarrow 10$	2
h	$0.5 \rightarrow 2$	0.5
θ	$-90 \rightarrow 90$	10

experiment, two datasets were extracted and used; dataset1 consists of 34 slices of one patient with low shape variations and dataset2 consists of 33 slices of the same patient with high shape variations. These slices were manually segmented to build the nonlinear shape prior and textural prior models as described in Section2 and Section3. We select 8 and 10 principle modes to represent the shape variation in dataset1 and dataset2 respectively. Figure 6 shows that every principle mode expresses a variation in some object parts. After we had built the shape and textural priors, we employed the proposed PSO segmentation technique on a set of slices of the patient used in the training stage and a set of novel slices for other patients. The resulting images shown in Figure 7 and Figure 8 illustrate the effectiveness of the proposed technique in liver segmentation from the CT images.

In the second experiment, a set of ten CT images of different patients was used for cross validation; nine patients were used for training and one patient was used for testing. Each CT image consists of about 170 slices stacked together and the liver fully appears in about 140 slices. In this experiment, a set of key frames were extracted from different patients at interval of 5 slices and all extracted frames were manually segmented. The level sets constructed from corresponding frames were used to build multi-shape and texture models. In this work, we use 27 slices to build each model and select 7 principle modes to represent the shape variations. Sample results of this experiment are shown in Figure 9 and Figure 10.

To validate the superiority of the proposed segmentation technique, five competitive techniques were utilized to segment the liver in the same set of slices and all results were compared. The first implemented technique is the active contour without edges [25] with a manual initialization inside the liver, the second technique performs the segmentation using the wavelet packet decomposition feature set and the fisher linear discriminate algorithm, the third technique utilizes the genetic algorithm (GA) to fit the pre-constructed shape model as proposed in [24], the fourth technique incorporate the linear shape priors of [12] in the segmentation framework, and The fifth technique is the technique proposed in [14] which incorporates nonlinear shape model and intensity-based model and it requires a manual initialization. Figure 11 shows the effectiveness of the proposed technique in the case of high shape variations , Figure 12 shows sample results of GA-based technique and Figure 13 demonstrates sample results of the fifth competitive technique. As shown in Figure 13, the balance between the shape model and the intensity-based model greatly influences the final results and keeping this balance manually is very difficult in the case of abdominal CT images. The goodness of fitness, G, of all techniques were computed for all datasets and compared in Table3, Table4 and Table5.

To calculate the goodness of fitness, we generate two binary masks to represent the manual and the computerized segmentation results. These masks have a value of 1 inside the object and a value of 0 outside. Then the goodness of fitness is calculated according to the following equation.

$$G = \frac{|Am \cap Aa|}{|Am \cup Aa|}, \tag{13}$$

where, Am represents the area of manually segmented object and Aa represents the area of automatically segmented object. A score of 1 represents a perfect match with the manual

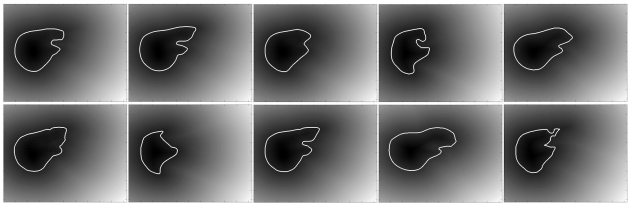

Fig. 6 The first 10 principle variation modes of dataset2, $\sqrt{\lambda_i}\alpha_i, i = 1, 2, \ldots, 10$ from left to right and up to down, the black contour represents the shape boundary.

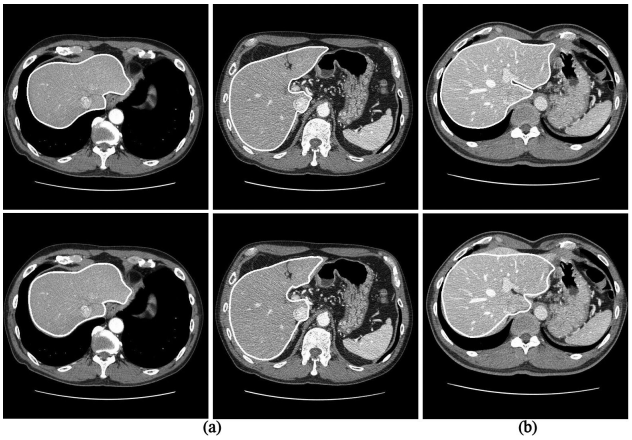

Fig. 7 Samples of the proposed technique results,first experiment-dataset1, (a) images for the patient used in training, (b) images of the other patients - the manual segmentation on the upper row and the automatic segmentation on bottom row.

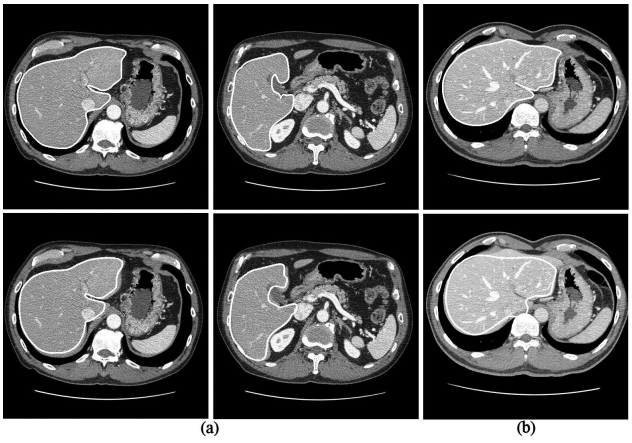

Fig. 8 Samples of the proposed technique results,first experiment-dataset2, (a) images for the patient used in training, (b) images of the other patients - the manual segmentation on the upper row and the automatic segmentation on bottom row.

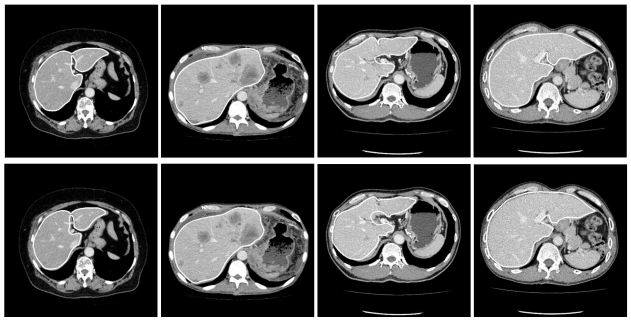

Fig. 9 Samples of The proposed technique results, the second experiment, on test slices extracted from the patients used in the training stage, the manual segmentation on the upper row and the results on the bottom row.

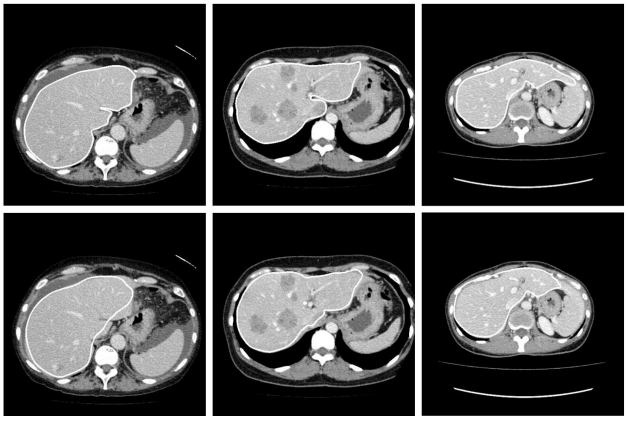

Fig. 10 Samples of The proposed technique results, the second experiment, on novel test slices extracted from the test patients, the manual segmentation on the upper row and the results on the bottom row.

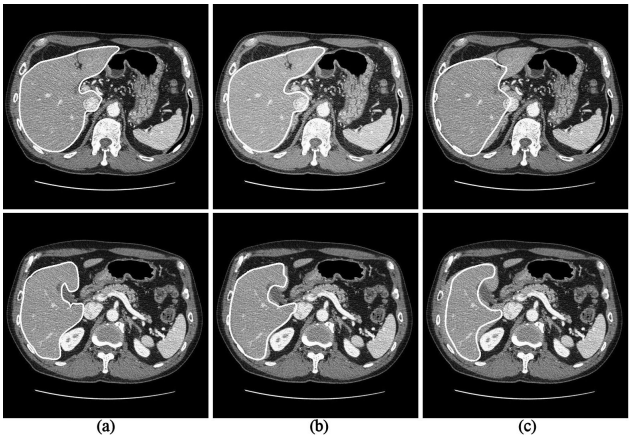

Fig. 11 Comparison of the results of incorporating linear and nonlinear shape priors in the segmentation framework, (a) manual segmentation, (b) nonlinear shape priors and (c) linear shape priors.

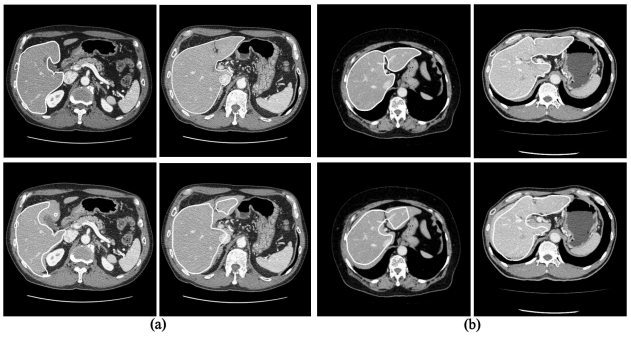

Fig. 12 Samples of genetic algorithm-based segmentation technique results, (a) the first experiment, (b) the second experiment, the manual segmentation on the upper row and the results on the bottom row.

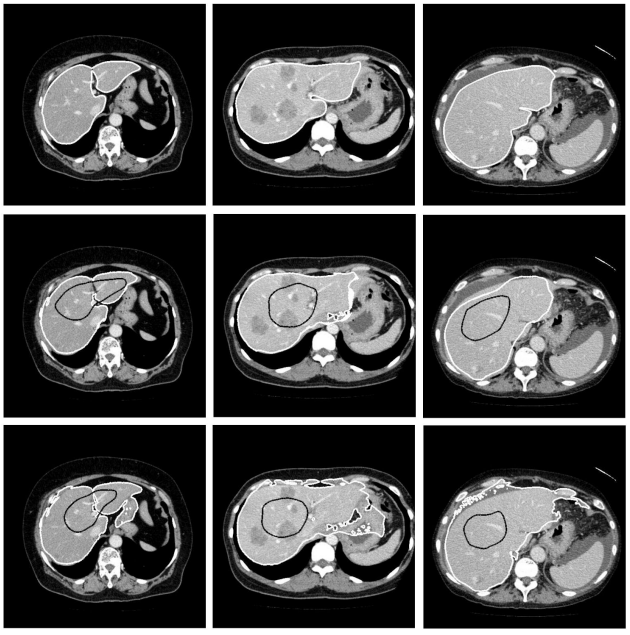

Fig. 13 Sample results of the framework proposed in [14], the upper row is the manual segmentation, the middle row is the best obtained results using a mixture of 40% of intensity-based model and 60% of shape model, and the bottom row is the results obtained using a mixture of 50% of intensity-based model and 60% of shape model, the black curve is the manual initialization and the white one is the final evolution result.

Table 3 Goodness of Fitness of the Final Segmentation Results (First experiment, dataset1).

Segmentation technique	Training Patient	Test Patients
The proposed Technique	0.95	0.88
Linear shape priors	0.94	0.83
Active contour without edges	0.70	0.75
Wavelet packet decomposition	0.52	0.45
GA-based technique	0.84	0.80
The technique proposed in [14]	0.94	0.85

segmentation.

7. Conclusion and Futute Work

In this work, the high level features extracted using the over-complete wavelet decomposition allows the technique to accurately discriminate the desired tissue. Also, the incorporation of nonlinear shape priors increases the ability to capture the desired object accurately. In addition, the utilization of the particle swarm optimization algorithm to adapt a region

Table 4 Goodness of Fitness of the Final Segmentation Results (First experiment, dataset2).

Segmentation technique	Training Patient	Test Patients
The proposed Technique	0.92	0.88
Linear shape priors	0.75	0.73
GA-based technique	0.80	0.75
The technique proposed in [14]	0.90	0.86

Table 5 Goodness of Fitness of the Final Segmentation Results (Second experiment).

Segmentation technique	Training Patients	Test Patients
The proposed Technique	0.96	0.93
Linear shape priors	0.92	0.88
Active contour without edges	0.72	0.74
Wavelet packet decomposition	0.50	0.48
GA-based technique [14]	0.89	0.83
The technique proposed in [14]	0.93	0.90

based level set function eliminates the need for deriving gradient of energy or solving complicated differential equations and it doesn't need level set re-initialization. Moreover, the PSO algorithm can efficiently explore the search space to converge to the desired object and its parameters can be easily adapted for any object.

In the future, we intend to enhance this PSO segmentation technique by employing the parallel PSO algorithm and utilize it for volume segmentation and visualization and as a primary step in automatic segmentation of liver tumors.

References

[1] A. Bartesaghi, and M. Nadar, "Segmentation of anatomical structure from DT-MRI", Proc. 3rd IEEE International Symposium on Biomedical Imaging: Nano to Macro, pp.61-64, April 2006.

[2] M. Jolly, and L. Grady, "3D general lesion segmentation in CT", Proc. 5th IEEE International Symposium on Biomedical Imaging: Nano to Macro , pp.796-799, May 2008.

[3] B. Reitinger, A. Bornik, R. Beichel, and D. Schmalstieg, "Liver surgery planning using virtual reality", Computer Graphics and Applications, IEEE , vol.26, no.6, pp.36-47, Nov.-Dec. 2006.

[4] W. Wieclawek, and E. Pietka, "Live-wire-based 3D segmentation method",Proc. 29th Annual International Conference of the IEEE Engineering in Medicine and Biology Society -EMBS 2007 , pp.5645-5648, Aug. 2007.

[5] R. Hult, "Grey-level morphology based segmentation of MRI of the human cortex" , Proc. 11th International Conference on Image Analysis and Processing, pp.578-583, Sep. 2001.

[6] C. Lee, P. Chung, and H. Tsai, "Identifying multiple abdominal organs from ct image series usinmg a multimodule contextual neural network and spatial fuzzy rules. IEEE Transaction on Information Technology in Biomedicine", vol.7, no.3, pp.208-217, 2003.

[7] D. Seghers, et al., "Model-based segmentation using Graph representations", Proc. the 11th international Conference on Medical Image Computing and Computer-Assisted intervention - Part I, New York, NY, USA, pp.393-400, Sep. 2008.

[8] P. Campadelli, and E. Casiraghi, "liver segmentation from CT scans: a survey", Proc. the 7th international Workshop on Fuzzy Logic and Applications: Applications of Fuzzy Sets theory ,Camogli, Italy, pp.520-528, July 2007.

[9] J. S. Osher, R. P. Fedkiw,Level Set Methods and Dynamic Implicit Surfaces, Springer-Verlag, New York, 2003 .

[10] L. Ning ,L. Miaomiao, and L. Youfu, "Image segmentation algorithm using watershed transform and level set method", Proc. IEEE International Conference on Acoustics, Speech and Signal Processing, pp.613-616, April 2007.

[11] A. Oktay, Y. Akgul, "Prior information based segmentation: A 3D level set surface matching approach", Proc. 23rd International Symposium on Computer and Information Sciences, pp.1-6, Oct. 2008.

[12] A. Tasi, et al., "A Shape-Based Approach to the Segmentation of Medical Imagery Using Level Sets", IEEE transaction on medical imaging, vol.22, vo.2, pp.137-154, 2003.

[13] Y. Rathi, S. Dambreville, and A. Tannenbaum, "Statistical shape analysis using kernel PCA", Proc. SPIE, Image Processing: Algorithms and Systems, Neural Networks, and Machine Learning, pp.425-432, Feb. 2006.

[14] S. Dambreville, Y. Rathi, and A. Tannenbaum, "A framework for image segmentation using shape models and kernel space shape priors", IEEE Transactions on Pattern Analysis and Machine Intelligence, vol.30, no.8, pp. 1385-1399, Aug. 2008.

[15] J. Kennedy, and R. Eberhart, "Particle Swarm Optimization", Proc. the IEEE international conferences on neural networks IV, pp.1942-1948, Nov./Dec. 1995.

[16] R. Hassan, B. Cohanim, and O. de Weck, "A comparison of particle swarm optimization and the genetic algorithm", Proc. 46th AIAA/ASME/ASCE/AHS/ASC Structures, Structural Dynamics, and Materials Conference, pp.1-13, April 2005.

[17] R. Poli, J. Kennedy, and T. Blackwell, "Particle swarm optimization: an overview", Springer Journal of Swarm Intelligence, Vol.1, pp.33-57, 2007.

[18] M. Clerc, Particle Swarm Optimization, ISTE Ltd, 2006.

[19] B. Schlkopf, A. Smola, K. Mller, "Nonlinear component analysis as a kernel eigenvalue problem", Neural Computation, vol.10, no.5, pp.1299-1319, Jul. 1998.

[20] C. de Boor, A Practical Guide to Splines, Springer-Verlag, New York, 1978.

[21] Y. Li, et al., "Segmentation of images using wavelet packet based feature set and clustering algorithm", International Journal of Information Technology, vol.11, no.7, pp.112-121, 2005.

[22] V. Franc, V. Hlavac, "Statistical Pattern Recognition Toolbox for Matlab", Prague, Czech: Center for Machine Perception, Czech Technical University, 2004.

[23] P. Arias, G. Randall, and G. Sapiro, Connecting the out-of-sample and pre-image problems in kernel methods", Proc. IEEE International Conference on Pattern Recognition, June 2007.

[24] P. Ghosh, and M. Michell, "Segmentation of medical images using a genetic algorithm", Proc. the 8th annual conference on Genetic and evolutionary computation, pp.1171-1178, July 2006.

[25] T. Chan, L. Vese, "Active Contour Without edges", IEEE transactions on image processing, vol.10, no.2, pp.266-277, Feb. 2001.

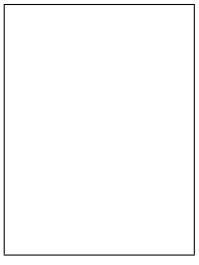

Ahmed Afifi was born in Menoufiya, Egypt, on January, 1980.He received the B.Sc. from the faculty of science and the M.Sc. from the faculty of computers and information, Menoufiya University, Egypt in 2000 and 2005, respectively. He is currently pursuing the doctoral degree at Chiba University, Chiba, Japan. His scientific interests include medical image analysis, pattern recognition, and optimization in vision.

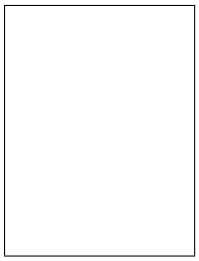

Toshiya Nakaguchi was born in Kobe, Japan, on April, 1975. He received the B.E., M.E., and Ph.D. degrees from Sophia University, Tokyo, Japan in 1998, 2000, and 2003, respectively. He was a research fellow supported by Japan Society for the Promotion of Science from April 2001 to March 2003. From 2006 to 2007, he was a research fellow in Center of Excellence in Visceral Biomechanics and Pain, in Aalborg Denmark, supported by CIRIUS, Danish Ministry of Education from 2006 to 2007. Currently, he is an Assistant Professor of imaging science at the Graduate School of Advanced Integration Science, Chiba University, Chiba Japan. His current research interests include the computer assisted surgery and medical training, medical image analysis, real-time image processing, and image quality evaluation.

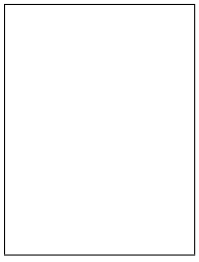

Norimichi Tsumura was born in Wakayama, Japan, on 3rd April 1967. He received the B.E., M.E. and D.E. in applied physics from Osaka University in 1990, 1992 and 1995, respectively. He moved to the Department of Information and Image Sciences, Chiba University in April 1995, as assistant professor. He is currently associate professor since 2002, and also researcher at PREST, Japan Science and Technology Corporation (JST). He was visiting scientist in University of Rochester from March 1999 to January 2000. He got the Optics Prize for Young Scientists (The Optical Society of Japan) in 1995, and Applied Optics Prize for the excellent research and presentation (The Japan Society of Applied Optics) in 2000. He received the Charles E. Ives award in 2002 from the IS&T. He is interested in the color image processing, computer vision, computer graphics and biomedical optics.

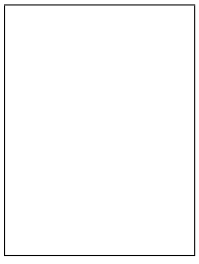

Yoichi Miyake has been professor of Chiba University since 1989. He received Ph.D. from Tokyo Institute of Technology in 1978. During 1978 and 1979, he was a post doctoral fellow of Swiss Federal Institute of Technology (ETHZ). In 1997, he was a guest professor of University of Rochester. He received Charles E Ives Award (paper award) from IS&T in 1991,2001 and 2005. He became a fellow of IS&T in 1995. He was named as Electronic Imaging Honoree of the year in 2000 from SPIE and IS&T. He became honorary member of IS&T in 2003. He published many books and original papers on the image processing, color science, image evaluations and he is known as a pioneer of spectral image processing. He was served as a president of SPSTJ (The Society of Photographic Science and Technology of Japan) from 2000 to 2002 and a vice president of IS&T (The Society for Imaging Science and Technology, USA) from 2000 to 2004. He was also served as a president of The Japanese Association of Forensic Science and Technology from 1998 to 1999. From 2003 to 2009, he was served as professor and director of Research Center for Frontier Medical Engineering in Chiba University. He is currently served as Research Professor in Chiba University.